

A lattice Boltzmann model for squirmers

Cite as: J. Chem. Phys. **150**, 144110 (2019); <https://doi.org/10.1063/1.5085765>

Submitted: 14 December 2018 . Accepted: 11 March 2019 . Published Online: 09 April 2019

Michael Kuron , Philipp Stärk, Christian Burkard, Joost de Graaf , and Christian Holm 



View Online



Export Citation



CrossMark

ARTICLES YOU MAY BE INTERESTED IN

[A kinetic-Monte Carlo perspective on active matter](#)

The Journal of Chemical Physics **150**, 144113 (2019); <https://doi.org/10.1063/1.5085828>

[Response of active Brownian particles to shear flow](#)

The Journal of Chemical Physics **150**, 144111 (2019); <https://doi.org/10.1063/1.5086495>

[Boundary conditions derived from a microscopic theory of hydrodynamics near solids](#)

The Journal of Chemical Physics **150**, 144104 (2019); <https://doi.org/10.1063/1.5088354>

The Journal
of Chemical Physics

2018 EDITORS' CHOICE

READ NOW!

A lattice Boltzmann model for squirmers

Cite as: J. Chem. Phys. 150, 144110 (2019); doi: 10.1063/1.5085765

Submitted: 14 December 2018 • Accepted: 11 March 2019 •

Published Online: 9 April 2019



Michael Kuron,^{1,a)} Philipp Stärk,¹ Christian Burkard,¹ Joost de Graaf,² and Christian Holm¹

AFFILIATIONS

¹Institute for Computational Physics, University of Stuttgart, Allmandring 3, 70569 Stuttgart, Germany

²Institute for Theoretical Physics, Center for Extreme Matter and Emergent Phenomena, Utrecht University, Princetonplein 5, 3584 CC Utrecht, The Netherlands

Note: This article is part of the Special Topic “Chemical Physics of Active Matter” in J. Chem. Phys.

a) Electronic mail: mkuron@icp.uni-stuttgart.de

ABSTRACT

The squirmer is a simple yet instructive model for microswimmers, which employs an effective slip velocity on the surface of a spherical swimmer to describe its self-propulsion. We solve the hydrodynamic flow problem with the lattice Boltzmann (LB) method, which is well-suited for time-dependent problems involving complex boundary conditions. Incorporating the squirmer into LB is relatively straightforward, but requires an unexpectedly fine grid resolution to capture the physical flow fields and behaviors accurately. We demonstrate this using four basic hydrodynamic tests: two for the far-field flow—accuracy of the hydrodynamic moments and squirmer-squirmer interactions—and two that require the near field to be accurately resolved—a squirmer confined to a tube and one scattering off a spherical obstacle—which LB is capable of doing down to the grid resolution. We find good agreement with (numerical) results obtained using other hydrodynamic solvers in the same geometries and identify a minimum required resolution to achieve this reproduction. We discuss our algorithm in the context of other hydrodynamic solvers and present an outlook on its application to multi-squirmer problems.

Published under license by AIP Publishing. <https://doi.org/10.1063/1.5085765>

I. INTRODUCTION

Directed motion, or motility, is of paramount importance to biology.¹ For example, it allows bacteria to move toward a food source² and fish to swim in formations that protect them from predators.³ In the presence of other bacteria, motility can lead to collective effects^{4–6} bearing resemblance of the schooling of fish or the swarming of birds, suggesting that the specifics of the propulsion, or even the length scale on which it occurs, have little effect on the overall behavior. Yet, we know that these two situations are drastically different from the perspective of interactions via the medium, which are tied to the way the organisms achieve propulsion.³

To experimentally better understand how the propulsion method affects the motion of an individual biological swimmer and how the motion affects the collective behavior of many biological swimmers together, artificial analogs have been developed. Realizations include catalytic^{7,8} and self-thermophoretic^{9,10} propulsion methods. These models have a well-defined geometrical shape and characterizable chemical properties, thus eliminating biological complications like shape changes or the beating of cilia. Yet, despite

their simplicity, they show the same kinds of collective effects as their biological counterparts.^{11,12}

Theoretical description of motility and the associated out-of-equilibrium phenomena is possible using models such as the one by Vicsek¹³ or the active Brownian particle (ABP) model.^{14,15} These approaches have been quite successful in qualitatively capturing the behaviors observed in nature. However, both neglect the hydrodynamic interactions mediated by the surrounding fluid, which can be important for microorganisms and their artificial counterparts.³ One way to overcome this limitation is the squirmer model.^{16,17} Here, the microswimmer is described as a spherical object with a simple inhomogeneous surface slip velocity, typically suspended in a Newtonian fluid. The squirmer model's long-ranged hydrodynamic interactions lead to reorientation similar to the Vicsek model, and, when complemented with a near-field repulsion, it accounts for the collisions that are captured by the ABP model. The squirmer model has proven to be an effective tool to model the effect of hydrodynamics in suspensions of both bacteria and man-made swimmers.^{18–20}

In this paper, we implement the squirmer model numerically using the lattice Boltzmann (LB) method,²¹ making use of the Ladd

moving boundary conditions.²² LB is in general a Navier-Stokes solver, but it can serve as a Stokes solver at the Reynolds numbers relevant to the systems considered in the present paper. The main advantages of LB over competing methods are momentum and mass conservation to machine precision, very low compressibility, and good obedience of the Stokes regime, as well as facile coupling to suspended particles. Furthermore, the algorithm scales to parallelize across large supercomputers²³ and is fully deterministic. Previous simulational studies of squirmers have not only used methods such as multi-particle collision dynamics^{24–26} (MPCD), finite element method^{27–29} (FEM), boundary element method^{30–33} (BEM), and Stokesian dynamics^{34–36} (SD), but also LB.^{18,37–39} We verify our implementation against well-known results from the literature^{30,32,40} and show that even for these basic cases several new things may be learned. Specifically, we study squirmers in bulk both individually and scattering off each other, as well as a squirmer oscillating between the two walls of a channel. Finally, we consider the interaction between a squirmer and an immobile spherical obstacle. We find that LB is well-capable of reproducing results obtained from other methods,^{30,32} but requires a higher resolution to reproduce accurate results than that is known from experience with passive particles in LB. This insight will enable us to accurately simulate dense suspensions of squirmers in the future and to study phenomena such as motility-induced phase separation.^{19,20,26,41}

The remainder of this paper is laid out as follows: In Sec. II, we discuss the squirmer model. In Sec. III, we introduce the relevant aspects of the LB method. In Secs. IV and V, we apply this numerical method to squirmers in bulk and interacting with boundaries, respectively. There, we also discuss implementation problems that arise and how our simulations compare to previous implementations, before we conclude in Sec. VI.

II. THE SQUIRMER MODEL

The near-field flow of a microswimmer is highly dependent on the specifics of its propulsion,⁴² so theoretical descriptions tend to resort to simple models capable only of producing the correct far-field behavior. One such model is the squirmer, initially introduced by Lighthill¹⁶ to explain swimming by oscillatory shape change. Blake¹⁷ later adapted it to describe the envelope of the ciliar motion of *Paramecium*, a microorganism. Both authors expand the flow around a spherical swimmer into spherical harmonics and discover that only the first two modes are needed to accurately capture the far-field flow. Most current squirmer applications further do away with any flow radially through the surface,³⁰ such that the ciliar motion on the surface of a sphere with radius R corresponds to a flow velocity boundary condition¹⁷

$$\mathbf{u}(\mathbf{r})|_{r=R} = \left(B_1 + B_2 \frac{\hat{\mathbf{e}} \cdot \mathbf{r}}{r} \right) \left(\frac{\hat{\mathbf{e}} \cdot \mathbf{r}}{r} \mathbf{r} - \hat{\mathbf{e}} \right) \quad (1)$$

in its rest frame, where \mathbf{r} is the position vector relative to the sphere's center, B_n are constants, and $\hat{\mathbf{e}}$ is the unit orientation vector of the sphere. Due to the small size of a microswimmer, a low Reynolds number approximation

$$\text{Re} = \frac{2\rho v_0 R}{\eta} \ll 1, \quad (2)$$

with the fluid density ρ , dynamic viscosity η , and the characteristic velocity v_0 may be made to the Navier-Stokes equations that govern the fluid flow. The resulting Stokes equations for hydrodynamics are given by

$$\eta \nabla^2 \mathbf{u}(\mathbf{r}) = -\nabla p(\mathbf{r}), \quad (3)$$

$$\nabla \cdot \mathbf{u}(\mathbf{r}) = 0, \quad (4)$$

where it is important to note that self-propulsion is force-free.^{43,44} Here, p refers to the pressure and ∇ , $\nabla \cdot$, and ∇^2 are the gradient, divergence, and Laplace operators, respectively. With the boundary condition of Eq. (1), one obtains the flow field^{17,30}

$$\begin{aligned} \mathbf{u}(\mathbf{r}) = & B_1 \frac{R^3}{r^3} \left(\frac{\hat{\mathbf{e}} \cdot \mathbf{r}}{r} \mathbf{r} - \frac{1}{3} \hat{\mathbf{e}} \right) + B_2 \left(\frac{R^4}{r^4} - \frac{R^2}{r^2} \right) \left(\frac{3}{2} \left(\frac{\hat{\mathbf{e}} \cdot \mathbf{r}}{r} \right)^2 - \frac{1}{2} \right) \frac{\mathbf{r}}{r} \\ & + B_2 \frac{R^4}{r^4} \frac{\hat{\mathbf{e}} \cdot \mathbf{r}}{r} \left(\frac{\hat{\mathbf{e}} \cdot \mathbf{r}}{r} \mathbf{r} - \hat{\mathbf{e}} \right) \end{aligned} \quad (5)$$

in the co-moving frame and sees that the squirmer moves with a velocity of

$$\mathbf{v}_0 = \frac{2}{3} B_1 \hat{\mathbf{e}} \quad (6)$$

in the laboratory frame.^{17,30} The dipolarity

$$\beta = \frac{B_2}{B_1} \quad (7)$$

is the ratio of the magnitudes of the second (force dipole, r^{-2} decay) and first mode (source dipole, r^{-3} decay). Note that the former always brings along a source quadrupole term (r^{-4} decay), which cannot be scaled independently. β describes the shape of the flow

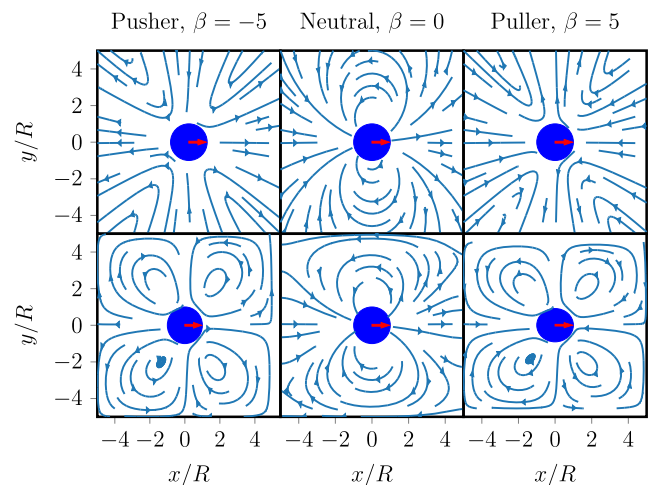


FIG. 1. Top: the analytical flow fields of squirmers with $\beta \in \{-5, 0, 5\}$ in an unbounded domain ($L = \infty$). The red arrows indicate that the squirmer is oriented such that it moves to the right. Bottom: the flow fields of the same squirmers at a resolution of $R = 8$ as obtained via LB in a cubic box of length $L = 10R$ with PBCs. As one can see, the flow field is heavily influenced by the PBCs. The analytical solution can also be determined for PBCs and looks indistinguishable from the LB flow fields.

field and its sign distinguishes between different kinds of swimmers. In the far field, a pusher like the *Escherichia coli* bacterium⁴⁵ ($\beta < 0$) pushes away fluid at its front and back and pulls fluid in from its sides, while pullers such as the *Chlamydomonas reinhardtii* alga⁴² ($\beta > 0$) pull fluid inward from the front and back and pushes it toward its sides. *Paramecium*,⁴⁶ as a neutral swimmer with $\beta = 0$, has a different far-field behavior and moves fluid from its front to its back. The three types of swimmer are illustrated in Fig. 1.

III. NUMERICAL METHOD

To account for the above hydrodynamics numerically, we employ the LB method.²¹ Instead of solving the Stokes equations (3) and (4) directly, this method solves the Boltzmann transport equation which obeys the same conservation laws and describes the evolution of a function $f(\mathbf{r}, \mathbf{v}, t)$. This is the system's single-particle phase space probability distribution, giving the probability of finding a fluid molecule with velocity \mathbf{v} at position \mathbf{r} and time t . The LB method linearizes the relaxation of f to its Maxwellian equilibrium, while discretizing space on a cubic lattice with the lattice constant a_{grid} and time in steps of τ . Only a finite set of velocities \mathbf{c}_i is permitted, specifically those that allow probability to flow between neighboring cells, making the populations $f_i(\mathbf{r}, t) := f(\mathbf{r}, \mathbf{c}_i, t)$. We choose the D3Q19 velocity set (3 dimensions and 18 face and edge neighbors). Throughout this paper, we use the two relaxation time (TRT) collision operator⁴⁷ which relaxes symmetric and antisymmetric linear combinations of f_i separately. The symmetric relaxation corresponds to stress relaxation with the relaxation time λ_e determining the viscosity. The antisymmetric relaxation gives a second relaxation time λ_o as a free parameter that can be used to improve the faithfulness of the boundary conditions.⁴⁸ The resulting LB equation is

$$f_i(\mathbf{r} + \mathbf{c}_i\tau, t + \tau) = f_i(\mathbf{r}, t) - \lambda_e(f_i^+ - f_i^{\text{eq}+}) - \lambda_o(f_i^- - f_i^{\text{eq}-}) \quad (8)$$

with

$$f_i^\pm(\mathbf{r}, t) = \frac{1}{2}(f_i(\mathbf{r}, t) \pm f_{\bar{i}}(\mathbf{r}, t)), \quad (9)$$

$$f_i^{\text{eq}\pm}(\mathbf{r}, t) = \frac{1}{2}(f_i^{\text{eq}}(\mathbf{r}, t) \pm f_{\bar{i}}^{\text{eq}}(\mathbf{r}, t)), \quad (10)$$

$$f_i^{\text{eq}}(\mathbf{r}, t) = w_i\rho(\mathbf{r}, t)\left(1 + 3\mathbf{c}_i \cdot \mathbf{u}(\mathbf{r}, t) + \frac{1}{6}(\mathbf{c}_i \cdot \mathbf{u}(\mathbf{r}, t))^2 - \frac{1}{6}u(\mathbf{r}, t)^2\right), \quad (11)$$

$$\eta = \rho\left(\frac{1}{3\lambda_e} - \frac{1}{6}\right), \quad (12)$$

$$\lambda_o\lambda_e = \frac{3}{16}, \quad (13)$$

where f_i^\pm and $f_i^{\text{eq}\pm}$ are the symmetric (+) and antisymmetric (−) combinations of populations (f_i) and equilibrium populations (f_i^{eq}), respectively. The index \bar{i} is the one for which $-\mathbf{c}_i = \mathbf{c}_{\bar{i}}$. From the populations, the macroscopic flow fields can be recovered

$$\rho(\mathbf{r}, t) = \sum_{i=1}^{19} f_i, \quad (14)$$

$$\mathbf{u}(\mathbf{r}, t) = \sum_{i=1}^{19} f_i \mathbf{c}_i. \quad (15)$$

Note that Eqs. (8) and (15) do not need to be modified to account for a force^{49,50} as there is no external (nonhydrodynamic) force applied to the fluid. Fluid-particle interactions take place exclusively via boundary conditions.

Velocity boundary conditions such as the no-slip conditions we have on obstacles are introduced by reflecting populations that stream into the boundary back into the fluid. For nonzero velocity conditions, the reflected populations are shifted⁵¹ to obtain

$$f_i(\mathbf{r}_b + \tau\mathbf{c}_i, t + \tau) = f_{\bar{i}}(\mathbf{r}_b, t) + \frac{6\rho w_i \tau^2}{a_{\text{grid}}^2} \mathbf{c}_i \cdot \mathbf{v}_b, \quad (16)$$

where \mathbf{r}_b is a boundary node with the velocity \mathbf{v}_b and $\mathbf{r}_b + \tau\mathbf{c}_i$ is a fluid node.

If the boundary is allowed to move, the previous equation can be used as part of a particle coupling scheme introduced by Ladd.²² A swimmer with its geometric center at \mathbf{r} moving with velocity \mathbf{v} and angular velocity $\boldsymbol{\omega}$ has a surface velocity of

$$\mathbf{v}_b(\mathbf{r}_b, t) = \mathbf{v}(t) + \boldsymbol{\omega}(t) \times (\mathbf{r}_b - \mathbf{r}(t)) \quad (17)$$

in the lab frame. To complete the particle coupling, one needs to account for the momentum transfer due to the reflection by considering the force

$$\mathbf{F}_{\text{bb}}(t) = a_{\text{grid}}^3 \sum_{\mathbf{r}_b} \sum_{i=1}^{19} \mathbf{c}_i (f_i(\mathbf{r}_b, t) + f_{\bar{i}}(\mathbf{r}_b - \mathbf{c}_i\tau, t)) \quad (18)$$

and torque

$$\mathbf{T}_{\text{bb}}(t) = a_{\text{grid}}^3 \sum_{\mathbf{r}_b} \sum_{i=1}^{19} (\mathbf{r}_b - \mathbf{r}) \times \mathbf{c}_i (f_i(\mathbf{r}_b, t) + f_{\bar{i}}(\mathbf{r}_b - \mathbf{c}_i\tau, t)) \quad (19)$$

on the particle. Unlike Ladd's original algorithm,²² we do not average $\mathbf{F}_{\text{bb}}(t)$ and $\mathbf{T}_{\text{bb}}(t)$ over two time steps. This is generally only necessary if oscillations in these quantities are observed between consecutive time steps. Note that the net force and torque of the system is still zero as required of a microswimmer:⁵² the above force and torque just account for momentum transferred between fluid and particle.

One further detail of the moving boundary scheme is that cells transition between fluid and boundary over time. Aidun *et al.*⁵³ suggested to set the populations of a cell to zero when it is converted to boundary and to set the populations to their equilibrium value (based on the swimmer's velocity and the average density of surrounding fluid cells) when it is converted back to fluid. This violates instantaneous mass conservation, but is unproblematic as average mass is conserved. To conserve momentum, destruction and creation of populations at position \mathbf{r}_f need to be accounted for as a force

$$\mathbf{F}_c(t) = \pm \frac{1}{\tau} \sum_{i=1}^{19} f_i(\mathbf{r}_f, t) \mathbf{c}_i \quad (20)$$

on the swimmer. Further enhancements of the moving-boundary method are reviewed in Ref. 54.

In Sec. V B, we include a short-range repulsion between pairs of swimmers, as well as between swimmer-obstacle pairs, in addition

to the hydrodynamic forces of Eqs. (18) and (20). This is a smooth approximation to a hard-core repulsion, as introduced by Weeks, Chandler, and Andersen,⁵⁵

$$F_{\text{WCA}}(r) = 24\epsilon \left(\frac{2}{r} \left(\frac{\sigma}{r} \right)^{12} - \frac{1}{r} \left(\frac{\sigma}{r} \right)^6 \right) + \epsilon \quad (21)$$

with the surface-to-surface distance r , cut-off radius $2^{1/6}\sigma$, and magnitude ϵ .

Based on the sum of the forces of Eqs. (18)–(21), the swimmer's trajectory can be integrated using a standard symplectic Euler scheme. We employ the waLBerla simulation framework,²³ which implements the TRT LB algorithm of Eq. (8) and also includes a rigid-body integrator⁵⁶ and the moving boundaries of Eqs. (17)–(20). The same method has been implemented in previous studies by other authors.^{18,37,39,57,58}

IV. FAR-FIELD RESULTS

In this section, we describe the simple validation tests for our numerical implementation. We start with the far field, where we simulate the bulk flow field and interactions between two squirmers. Next, we consider a squirmer confined in a narrow cylindrical tube, and we conclude with the scattering of a squirmer off a spherical obstacle.

A. Squirmers in bulk

In Fig. 1, we show the flow fields of the three types of squirmer in bulk fluid. As LB is typically used with periodic boundary conditions (PBCs), a direct comparison to Eq. (5) would require either an extremely large simulation domain in LB or incorporating the effect of the periodic images into the analytical solution.^{59,60} The latter would require an Ewald summation approach,^{35,61} but can be approximated by summing over a spherical shell of periodic images. The largest differences between this approximate periodic analytical solution and the LB solution are found at $\pm 45^\circ$ from \hat{e} , where the flow magnitude is small. Ignoring these regions, the mean error is around 8% at a resolution of $R = 8$. Both of these deviations can be attributed to discretization errors. As we will discuss below, R (in units of the lattice spacing) needs to have a certain minimal value to avoid more severe discretization artifacts.

Figure 1 was obtained at a resolution of 8 cells per squirmer radius. Since we use lattice units, this corresponds to $R = 8$. In moving-boundary simulations of passive spheres, one typically aims for a resolution of $R \approx 4$ which provides sufficient accuracy while minimizing computational effort.⁶² In literature, resolutions around $R = 8$ are often used for squirmers,^{37,57,58} but usually not explicitly justified. Some authors^{18,39,63} do use smaller resolutions around $R = 3$, which for squirmers appears to only give usable results in the authors' specific case without preferred direction. We find that resolutions below a value of $R \approx 6$ lead to strong oscillations in the flow field, causing an alternating velocity pattern along the direction in which the squirmer moves; see Fig. 2. As seen in Fig. 3, the magnitude of the oscillation increases over time, suggesting a self-reinforcing numerical artifact. While at short times, the true flow can still be obtained by averaging over the oscillation, after several million time steps, they become so strong that the true flow is almost

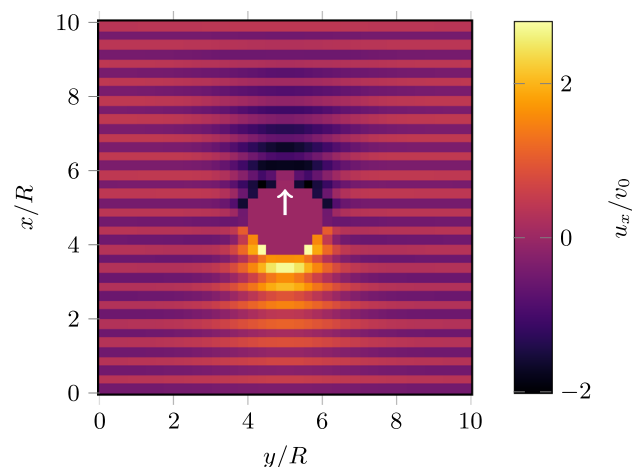


FIG. 2. Visualization of the deteriorated flow field after simulating a squirmer of radius $R = 4$ in a box of length $L = 10$ for $T = 1.5 \times 10^5 \Delta t$. u_x , the x-component of the fluid velocity, is shown in the xy -plane and normalized by the squirmer speed v_0 . The arrow shown in grey indicates the squirmers orientation.

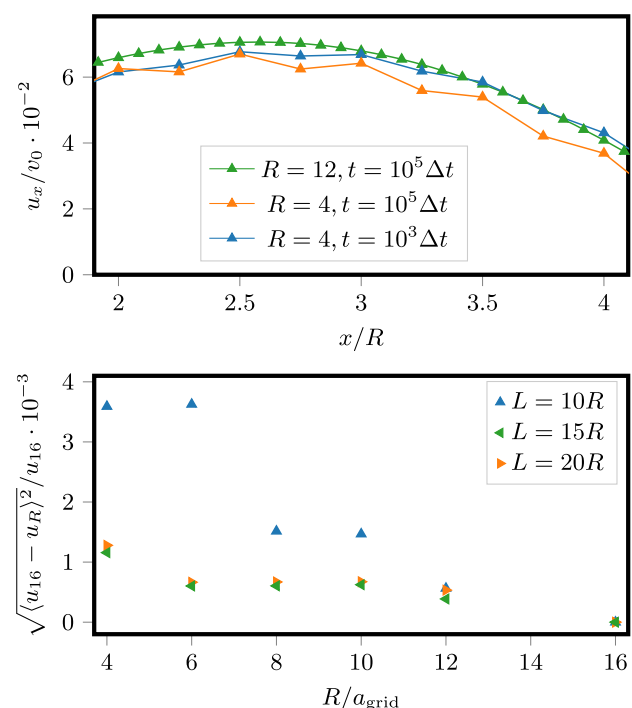


FIG. 3. Top: flow speed $u_x(x\hat{e}_x)$, normalized by the squirmer speed v_0 , along the x -axis for $L = 10R$. For high resolutions ($R = 12$), the curve is smooth, while for low resolutions ($R = 4$), an alternating pattern of faster and slower cells is visible that grows more distinct over time, matching the stripes in Fig. 2. Bottom: Standard deviation of the velocity error obtained by comparing the flow field u_R at a radius R to that of a high-resolution simulation ($R = 16$) for the entire simulation domain. Larger values correspond to more inhomogeneous errors, i.e., the development of the alternating pattern described in the main text. Time $t = 1000$ and different box sizes $L \in \{10R, 15R, 20R\}$ are shown. The difference between $L = 15R$ and $L = 20R$ can be attributed to our error fitting procedure.

completely obscured. Eventually, the simulation becomes unstable because LB does not accurately handle strong velocity gradients like those in Fig. 2 well. This phenomenon is most often seen in systems with a preferred direction. Alarcón *et al.*,^{18,39} for example, did not see this effect because they have dense suspensions of squirmers that continuously change their orientations. For comparison, in MPCD, squirmer radii of three collision cells, each of which containing an average of 80 MPCD particles, are reported to have been used.²⁶ Since the computational effort for an LB cell and for an MPCD particle are on the same order of magnitude, the resolution requirement can be considered to be similar for LB and MPCD.

In Fig. 4, we show how the squirmer's speed v depends on the resolution as given by the squirmer's radius R and on the box length L . In analytical theory and in LB in the infinite-resolution limit, this speed equals the squirmer parameter v_0 from Eq. (6). In Fig. 4, we observe that we approach v_0 from below as resolution increases. At $R = 6$, we are already within 0.5% of the correct value (0.2% at $R = 12$) for the largest box size. For the smaller box sizes, the interaction of the squirmer with its periodic images decreases the velocity slightly. For comparison, the same data is also plotted for a passive sphere being dragged through a resting fluid at otherwise identical parameters. The periodicity effect is much weaker for the squirmer than for the passive sphere since the latter's flow is monopolar to leading order and thus decays more slowly than the squirmer's. Despite the seemingly good agreement of the observed squirmer velocity with the prescribed squirmer velocity even for small resolutions, the stripe pattern discussed in the previous paragraph massively modifies the flow field, to the extent that simulations at small resolutions simply give no meaningful results.

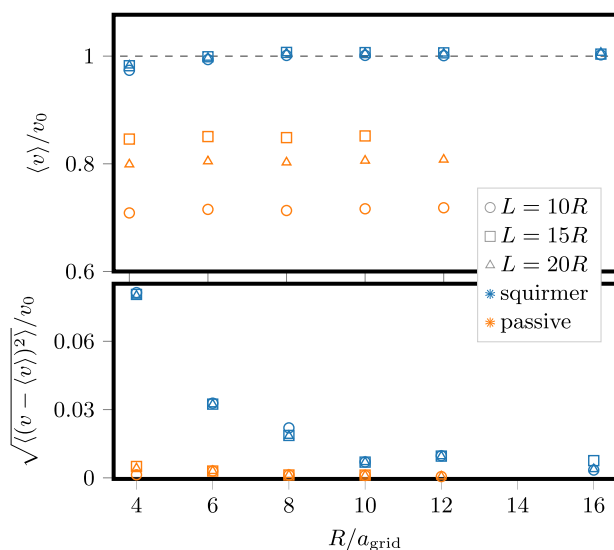


FIG. 4. Top: A squirmer's (orange) and a passive sphere's (blue) mean velocity $\langle v \rangle$, normalized by the expected bulk speed v_0 , as a function of the resolution of the squirmer/passive sphere. Bottom: Normalized variance of the respective bodies velocities indicating the spread around the mean velocity. The resolution is given by the radius R in lattice units. We show results for three box sizes as given by the edge length L , also in lattice units.

While the squirmer moves across the lattice, some variation in its speed is expected due to the sphere being composed of discrete cubes. As expected, Fig. 4 shows that the variation decreases with resolution; however, the variation is much larger than that for the equally-resolved passive sphere dragged through the fluid. The latter can be attributed to the cause of the motion—the squirmer is dragged along by the flow its own surface causes—and to the fact that this surface is significantly affected by the slight changes in the number of cells occupied by a sphere as it moves. For a graphical explanation of this problem, see Ref. 64, where we introduced a solution to a related problem for an electrophoretically driven particle. For the squirmer, an approach based on the method of Noble and Torczynski⁶⁵ might prove useful.

B. Interaction between two squirmers

Now that we have confirmed that our LB implementation is capable of producing the correct flow around a squirmer, we check that a squirmer correctly reacts to the flow produced by another squirmer. Here, we approximated the situation first considered by Ishikawa *et al.*,³⁰ who positioned two squirmers facing opposite each other, separated by a distance of $12R$ and spaced apart laterally by varying distances d . They solved for the trajectories using BEM, which assumes an infinite fluid domain size and discretizes the squirmers' surfaces. In our LB calculations, we used a squirmer radius of $R = 9$ and a cubic, periodic simulation domain with edge length $L = 250$ to approximate the bulk calculation of Ref. 30. Figure 5 shows the resulting trajectories and those of Ref. 30. There is good agreement, and our trajectories are considerably smoother than those given by Ishikawa *et al.* Part of the deviations can be attributed to the use of PBCs in our simulation,⁶⁶ the increased

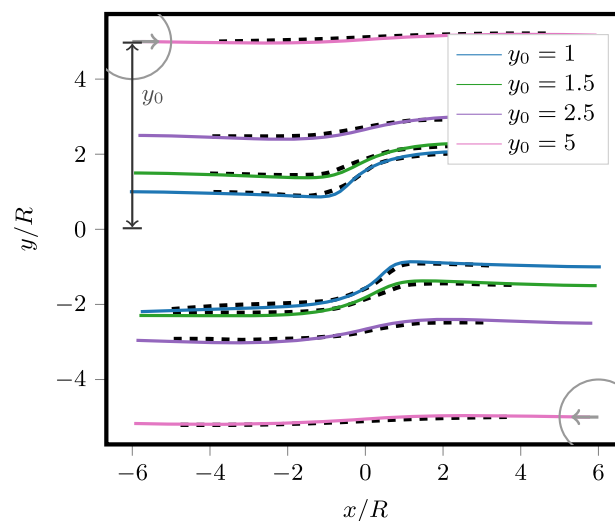


FIG. 5. Trajectories of two squirmers with $\beta = 5$ passing each other. The initial configuration is specified by the initial lateral separation $d = 2y_0$ and the separation in the direction of their original orientation. The results of Ref. 30 are shown as dashed lines. Our LB simulations are performed for squirmers with $R = 9$ in a periodic box of length $L = 250$.

smoothness is mostly related to the advancement in computational performance since 2006 and not an intrinsic issue with BEM. It is worth noting that we have used a far coarser resolution for our squirmers than used by Ishikawa *et al.* because we also need to discretize the entire fluid volume, while BEM only discretizes the surface. The good match between the much finer BEM resolution and our LB results is promising for simulations at much higher squirmer volume fractions, where we can reasonably expect to be able to maintain our current resolution and thus keep roughly the same simulation speed.

V. NEAR-FIELD RESULTS

Now that we have determined the resolution required for an accurate simulation and checked that two squirmers interact with each other correctly, we can investigate systems where the near field plays a dominant role.

A. Squirmer in a round tube

LB does not make use of the method of reflections to capture the effect of solid/no-slip boundaries and therefore can accurately reproduce the near-field flow when squirmers approach obstacles closer than their diameter. Note that we do not include lubrication corrections,^{35,62} which would be necessary to accurately capture the flow between two objects that are spaced less than one lattice constant apart. Keeping this in mind, we can now perform simulations where the near-field flow plays a role. Zhu *et al.*³² studied a neutral ($\beta = 0$) squirmer oscillating in a tube with circular diameter $D = 20R/3$ and length $L = 3\pi R$ with PBCs only along its length, starting from different distances y_0 to the boundary and an initial orientation parallel to the symmetry axis.

The trajectories we obtain are compared to the results from that publication in Fig. 6. Both the oscillation amplitude and the period match to within 3% of the literature value. The reorientation of the squirmer when it is near the wall is a near-field effect, so the agreement confirms that our LB method sufficiently captures it. Since Zhu *et al.*³² used BEM with local mesh refinement^{30,46} when squirmer and wall are near contact, they capture near-field effects more accurately than LB does at the resolution we used. This explains the slight deviations in the trajectories of Fig. 6, but the good agreement confirms that the system is rather robust to these differences. To obtain equally good results in LB at manageable computational effort, one would need to resort to an adaptive grid resolution.⁶⁷

B. Scattering off and orbiting around a stationary spherical obstacle

The last system we consider is that of a single squirmer scattering off or orbiting around a stationary spherical obstacle with radius A . Spagnolie *et al.*⁴⁰ have examined how force dipole swimmers interact with such an obstacle and found that, depending on the value of β and the ratio A/R , the swimmer may either orbit around or scatter off the obstacle. Here, we compare to their results using our LB squirmer. However, there are some notable differences between our method and the calculation by Spagnolie *et al.* which we will briefly address in the following.

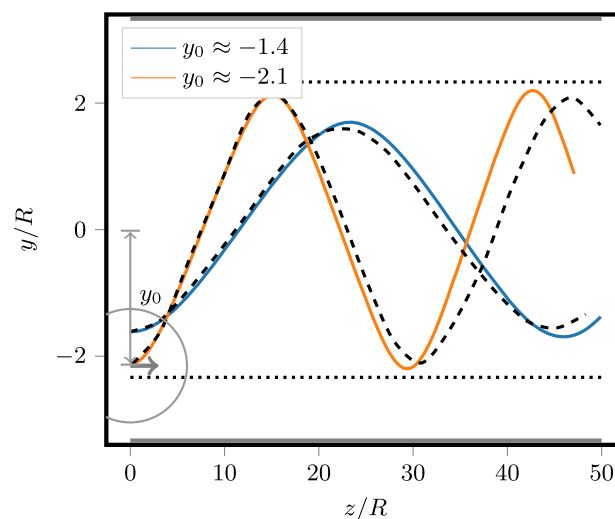


FIG. 6. Trajectories of squirmers ($R = 9$) with different initial displacements y_0 inside a tube of length $L = 3\pi R$ and circular diameter $D = 20R/3$, compared to the results of Ref. 32, which simulates the equivalent system using BEM. These are shown using black dashes. The dotted lines indicate the point of closest approach before the squirmer touches the boundary, which itself is marked using the grey lines at the top and bottom of the plot. Also shown: the location of the squirmer and its initial orientation in the case of $y_0 \approx -2.1$.

The force dipole is the slowest-decaying mode contained in the squirmer [Eq. (5)], so the far field agrees between our and their point-dipole approximation. However, close to the obstacle a far-field description is not sufficient to account for the finite size of a microswimmer. In our LB squirmer simulations, we do account for this effect, so deviations are expected with respect to the result of Ref. 40. Even if $|\beta|$ is chosen sufficiently large for the force dipole to dominate, qualitative agreement is only expected to a certain extent: since squirmers also contain a quadrupolar contribution, see Eq. (5), their behavior near surfaces is altered compared to a pure dipole.^{68–70} In addition to this hydrodynamic effect, there is a difference in the contact potential: We use a short-ranged WCA repulsion [Eq. (21)], while Ref. 40 uses a hard-core repulsion; the effect of this should be less pronounced than that of the addition of higher-order hydrodynamic moments. Finally, we would like to note that Chamolly *et al.*³⁶ studied a similar system, using actual squirmers instead of dipoles and a short-range repulsion that is softer than our WCA. However, they use SD,^{35,71} a far-field-only hydrodynamics solver (for $d \gg R$), combined with lubrication corrections^{35,72} (for $d \ll R$), meaning that near-field interactions ($\mathcal{O}(d) \approx \mathcal{O}(R)$) are not dealt with. Because Chamolly *et al.* only studied squirmers in high-volume fraction periodic crystals, we have excluded their results from our comparison.

In Fig. 7, we present the critical obstacle sizes A/R for different β ; below this curve, the squirmers scatter and above they orbit. Reference data from Ref. 40 is also shown, but needs to be considered with care since the model differs significantly in the ways discussed above. Furthermore, our LB model is only capable of relatively small A/R ratios as a constant resolution is used throughout the simulation domain, which makes the computational effort scale like $\mathcal{O}(A^3)$. To extend our results into the realm of parameters studied by

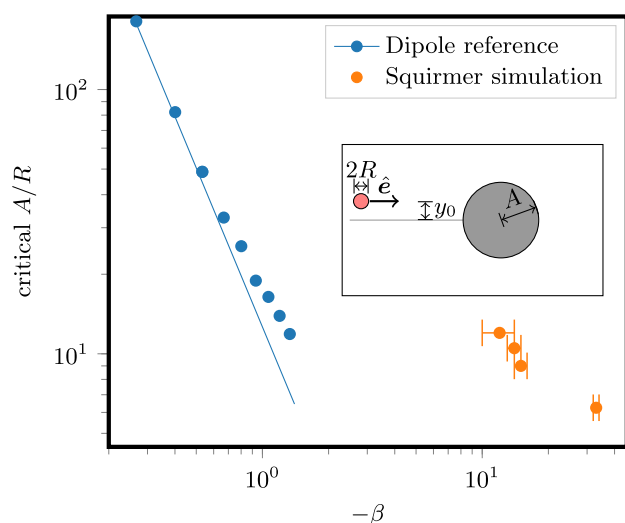


FIG. 7. Critical obstacle size A/R below which the squirmer scatters and above which it orbits, as a function of β , including error bars. The data shown in blue is extracted from Ref. 40 for force dipole pushers; the blue line is an analytical solution given there for small $|\beta|$. The inset schematically shows the system under investigation: a squirmer of radius R swims with a small offset y_0 above the x -axis towards the spherical obstacle of radius A .

Spagnolie *et al.*, an adaptive grid resolution⁶⁷ would be helpful. To obtain our figure, simulations at various values A and β are started with the squirmer of radius $R = 8$ positioned such that it moves radially toward the obstacle. In practice, one needs to break the symmetry by angling the trajectory slightly instead of using a perfectly radial one. While such an offset angle influences the angle by which a squirmer is scattered by the obstacle,⁴⁰ it does not affect the critical A/R , i.e., whether a squirmer enters into an orbit or not. A trajectory is considered to be an orbit if the squirmer revolves more than halfway around the obstacle, though we have performed simulations of a select number of situations to confirm that the squirmer indeed completes a full revolution and continues to orbit. To determine the exact position of the critical value, we performed bisection in A/R or β once at least one orbiting and one scattering parameter set had been found.

VI. CONCLUSION AND OUTLOOK

We have described in detail our implementation of a hydrodynamic squirmer model^{16,17} in an LB fluid dynamics solver, where we build upon a large body of literature on this topic.^{21,22,53} We have confirmed in four scenarios that our LB squirmer implementation can accurately reproduce signature features of the squirmer model, including (i) the analytic flow field around the squirmer, accounting for periodicity effects; (ii) the interaction between two squirmers, as originally obtained by Ishikawa *et al.*³⁰ using the boundary element method (BEM); (iii) the oscillation of a squirmer in a cylindrical tube as studied originally using BEM by Zhu *et al.*³² (iv) the scattering and orbiting of a squirmer around a spherical obstacle. This problem was analyzed theoretically by Spagnolie *et al.*⁴⁰ for a point-like force-dipole swimmer. Our squirmer model can only probe smaller

size ratios, but yields qualitatively similar trends of scattering vs orbiting in a size regime beyond theirs.

Through our study, we have also demonstrated that the LB squirmer implementation is sensitive to discretization artifacts, more so than has been reported for passive particles. Throughout the literature, various values of the resolution of the squirmer are used. Here, we show that a refinement of at least 8 lattice cells for the radius of the squirmer is necessary to avoid numerical artifacts in the flow field. These artifacts are particularly pronounced in situations where there is persistent motion and may lead to severe numerical instabilities.

We have made our LB squirmer implementation available within the open-source software waLBerla,²³ which will make it possible for anyone to simulate large-scale systems containing many squirmers and complex boundary conditions. It should be noted that we have not incorporated lubrication corrections^{35,62} here, which will be a topic for further method development.

ACKNOWLEDGMENTS

We thank the Deutsche Forschungsgemeinschaft (DFG) for funding through the SPP 1726 “Microswimmers: from single particle motion to collective behavior” (Nos. HO1108/24-1 and HO1108/24-2). We are grateful to Alexander Chamolly for useful discussions and to Martin Bauer, Sebastian Eibl, Christian Godenschwager, Christoph Rettinger, and Florian Schornbaum for developing waLBerla and supporting us in using and extending it.

REFERENCES

- M. E. Cates, *Rep. Prog. Phys.* **75**, 042601 (2012).
- C. Hoell and H. Löwen, *Phys. Rev. E* **84**, 042903 (2011).
- M. C. Marchetti, J.-F. Joanny, S. Ramaswamy, T. B. Liverpool, J. Prost, M. Rao, and R. A. Simha, *Rev. Mod. Phys.* **85**, 1143 (2013).
- D. B. Kearns, *Nat. Rev. Microbiol.* **8**, 634 (2010).
- H. H. Wensink, J. Dunkel, S. Heidenreich, K. Drescher, R. E. Goldstein, H. Löwen, and J. M. Yeomans, *Proc. Natl. Acad. Sci. U. S. A.* **109**, 14308 (2012).
- J. Gachelin, A. Rousselet, A. Lindner, and E. Clement, *New J. Phys.* **16**, 025003 (2014).
- J. R. Howse, R. A. Jones, A. J. Ryan, T. Gough, R. Vafabakhsh, and R. Golestanian, *Phys. Rev. Lett.* **99**, 048102 (2007).
- A. Erbe, M. Zientara, L. Baraban, C. Kreidler, and P. Leiderer, *J. Phys.: Condens. Matter* **20**, 404215 (2008).
- H.-R. Jiang, N. Yoshinaga, and M. Sano, *Phys. Rev. Lett.* **105**, 268302 (2010).
- I. Buttinoni, G. Volpe, F. Kümmel, G. Volpe, and C. Bechinger, *J. Phys.: Condens. Matter* **24**, 284129 (2012).
- M. Ibele, T. E. Mallouk, and A. Sen, *Angew. Chem.* **121**, 3358 (2009).
- J. Palacci, S. Sacanna, A. P. Steinberg, D. J. Pine, and P. M. Chaikin, *Science* **339**, 936 (2013).
- T. Vicsek, A. Czirók, E. Ben-Jacob, I. Cohen, and O. Shochet, *Phys. Rev. Lett.* **75**, 1226 (1995).
- P. Romanczuk, M. Bär, W. Ebeling, B. Lindner, and L. Schimansky-Geier, *Eur. Phys. J.: Spec. Top.* **202**, 1 (2012).
- W. Ebeling, F. Schweitzer, and B. Tilch, *BioSystems* **49**, 17 (1999).
- M. Lighthill, *Commun. Pure Appl. Math.* **5**, 109 (1952).
- J. Blake, *J. Fluid Mech.* **46**, 199 (1971).
- F. Alarcón and I. Pagonabarraga, *J. Mol. Liq.* **185**, 56 (2013).
- G. Gonnella, D. Marenduzzo, A. Suma, and A. Tiribocchi, *C. R. Phys.* **16**, 316 (2015).

- ²⁰A. Zöttl and H. Stark, *Phys. Rev. Lett.* **112**, 118101 (2014).
- ²¹G. R. McNamara and G. Zanetti, *Phys. Rev. Lett.* **61**, 2332 (1988).
- ²²A. J. C. Ladd, *J. Fluid Mech.* **271**, 285 (1994).
- ²³C. Godenschwager, F. Schornbaum, M. Bauer, H. Köstler, and U. Rüde, in *Proceedings of the International Conference on High Performance Computing, Networking, Storage and Analysis* (Association for Computing Machinery, 2013), p. 35.
- ²⁴M. T. Downton and H. Stark, *J. Phys.: Condens. Matter* **21**, 204101 (2009).
- ²⁵M. Theers, E. Westphal, G. Gompper, and R. G. Winkler, *Soft Matter* **12**, 7372 (2016).
- ²⁶M. Theers, E. Westphal, K. Qi, R. G. Winkler, and G. Gompper, *Soft Matter* **14**, 8590–8603 (2018).
- ²⁷L. Zhu, E. Lauga, and L. Brandt, *Phys. Fluids* **24**, 051902 (2012).
- ²⁸N. Aguilon, A. Decoene, B. Fabrèges, B. Maury, and B. Semin, in *ESAIM: Proceedings* (EDP Sciences, 2012), Vol. 38, pp. 36–53.
- ²⁹M. De Corato and G. D'Avino, *Soft Matter* **13**, 196 (2017).
- ³⁰T. Ishikawa, M. Simmonds, and T. Pedley, *J. Fluid Mech.* **568**, 119 (2006).
- ³¹K. Ishimoto and E. A. Gaffney, *Phys. Rev. E* **88**, 062702 (2013).
- ³²L. Zhu, E. Lauga, and L. Brandt, *J. Fluid Mech.* **726**, 285 (2013).
- ³³W. Uspal, M. Popescu, S. Dietrich, and M. Tasinkevych, *Soft Matter* **11**, 6613 (2015).
- ³⁴T. Ishikawa and T. Pedley, *Phys. Rev. Lett.* **100**, 088103 (2008).
- ³⁵T. Ishikawa, J. Locsei, and T. Pedley, *J. Fluid Mech.* **615**, 401 (2008).
- ³⁶A. Chamolly, T. Ishikawa, and E. Lauga, *New J. Phys.* **19**, 115001 (2017).
- ³⁷J. S. Lintuvuori, A. T. Brown, K. Stratford, and D. Marenduzzo, *Soft Matter* **12**, 7959 (2016).
- ³⁸I. Llopis and I. Pagonabarraga, *J. Non-Newtonian Fluid Mech.* **165**, 946 (2010).
- ³⁹F. Alarcón, C. Valeriani, and I. Pagonabarraga, *Soft Matter* **13**, 814 (2017).
- ⁴⁰S. E. Spagnolie, G. R. Moreno-Flores, D. Bartolo, and E. Lauga, *Soft Matter* **11**, 3396 (2015).
- ⁴¹M. E. Cates and J. Tailleur, *Annu. Rev. Condens. Matter Phys.* **6**, 219 (2015).
- ⁴²K. Drescher, R. Goldstein, N. Michel, M. Polin, and I. Tuval, *Phys. Rev. Lett.* **105**, 168101 (2010).
- ⁴³T. Ishikawa, *J. R. Soc., Interface* **6**, 815 (2009).
- ⁴⁴E. Lauga and T. R. Powers, *Rep. Prog. Phys.* **72**, 096601 (2009).
- ⁴⁵K. Drescher, J. Dunkel, L. Cisneros, S. Ganguly, and R. Goldstein, *Proc. Natl. Acad. Sci. U. S. A.* **108**, 10940 (2011).
- ⁴⁶T. Ishikawa and M. Hota, *J. Exp. Biol.* **209**, 4452 (2006).
- ⁴⁷I. Ginzburg, F. Verhaeghe, and D. d'Humières, *Commun. Comput. Phys.* **3**, 427 (2008).
- ⁴⁸I. Ginzburg, F. Verhaeghe, and D. d'Humières, *Commun. Comput. Phys.* **3**, 519 (2008).
- ⁴⁹Z. Guo, C. Zheng, and B. Shi, *Phys. Rev. E* **65**, 046308 (2002).
- ⁵⁰H. Huang, M. Krafczyk, and X. Lu, *Phys. Rev. E* **84**, 046710 (2011).
- ⁵¹Q. Zou and X. He, *Phys. Fluids* **9**, 1591 (1997).
- ⁵²E. Purcell, *Am. J. Phys.* **45**, 3 (1977).
- ⁵³C. K. Aidun, Y. Lu, and E.-J. Ding, *J. Fluid Mech.* **373**, 287 (1998).
- ⁵⁴C. Rettinger and U. Rüde, *Comput. Fluids* **154**, 74 (2017).
- ⁵⁵J. D. Weeks, D. Chandler, and H. C. Andersen, *J. Chem. Phys.* **54**, 5237 (1971).
- ⁵⁶J. Götz, K. Iglberger, C. Feichtinger, S. Donath, and U. Rüde, *Parallel Comput.* **36**, 142 (2010).
- ⁵⁷Z. Shen, A. Würger, and J. S. Lintuvuori, *Soft Matter* **15**, 1508 (2019).
- ⁵⁸Z. Shen, A. Würger, and J. S. Lintuvuori, *Eur. Phys. J. E* **41**, 39 (2018).
- ⁵⁹J. de Graaf and J. Stenhammar, *J. Fluid Mech.* **811**, 487 (2017).
- ⁶⁰T. C. Adhyapak and S. Jabbari-Farouji, *J. Chem. Phys.* **149**, 144110 (2018).
- ⁶¹J. F. Brady, R. J. Phillips, J. C. Lester, and G. Bossis, *J. Fluid Mech.* **195**, 257 (1988).
- ⁶²N.-Q. Nguyen and A. Ladd, *Phys. Rev. E* **66**, 046708 (2002).
- ⁶³I. Pagonabarraga and I. Llopis, *Soft Matter* **9**, 7174 (2013).
- ⁶⁴M. Kuron, G. Rempfer, F. Schornbaum, M. Bauer, C. Godenschwager, C. Holm, and J. de Graaf, *J. Chem. Phys.* **145**, 214102 (2016).
- ⁶⁵D. Noble and J. Torczynski, *Int. J. Mod. Phys. C* **9**, 1189 (1998).
- ⁶⁶J. de Graaf and J. Stenhammar, *Phys. Rev. E* **95**, 023302 (2017).
- ⁶⁷F. Schornbaum and U. Rüde, *SIAM J. Sci. Comput.* **38**, C96 (2016).
- ⁶⁸J. de Graaf, A. J. Mathijssen, M. Fabritius, H. Menke, C. Holm, and T. N. Shendruk, *Soft Matter* **12**, 4704 (2016).
- ⁶⁹A. J. Mathijssen, D. O. Pushkin, and J. M. Yeomans, *J. Fluid Mech.* **773**, 498 (2015).
- ⁷⁰X. Shen, H. C. Fu *et al.*, *Phys. Rev. E* **95**, 033105 (2017).
- ⁷¹J. F. Brady and G. Bossis, *Annu. Rev. Fluid Mech.* **20**, 111 (1988).
- ⁷²L. Durlinsky, J. F. Brady, and G. Bossis, *J. Fluid Mech.* **180**, 21 (1987).